

OPEN ACCESS

Leveraging Temperature-Dependent (Electro)Chemical Kinetics for High-Throughput Flow Battery Characterization

To cite this article: Eric M. Fell *et al* 2024 *J. Electrochem. Soc.* **171** 040501

View the [article online](#) for updates and enhancements.

You may also like

- [An Asymmetric Viologen-Based Negolyte with a Low Redox Potential for Neutral Aqueous Redox Flow Batteries](#)
Meisam Bahari, Gerald D. Watt and John N. Harb
- [Long-Term Stability of Ferri-/Ferrocyanide as an Electroactive Component for Redox Flow Battery Applications: On the Origin of Apparent Capacity Fade](#)
Eric M. Fell, Diana De Porcellinis, Yan Jing et al.
- [Leveraging Temperature-Dependent \(Electro\)Chemical Kinetics to Accelerate Redox Flow Battery Active Material Characterization](#)
Eric M. Fell and Michael J. Aziz



Your Lab in a Box!

The PAT-Tester-i-16: All you need for Battery Material Testing.

- ✓ All-in-One Solution with integrated Temperature Chamber!
- ✓ Cableless Connection for Battery Test Cells!
- ✓ Fully featured Multichannel Potentiostat / Galvanostat / EIS!

www.el-cell.com +49 40 79012-734 sales@el-cell.com

EL-CELL[®]
electrochemical test equipment





Leveraging Temperature-Dependent (Electro)Chemical Kinetics for High-Throughput Flow Battery Characterization

Eric M. Fell,¹ Thomas Y. George,¹ Yan Jing,² Roy G. Gordon,² and Michael J. Aziz^{1,z}

¹Harvard John A. Paulson School of Engineering and Applied Sciences, 29 Oxford Street, Cambridge, Massachusetts 02138, United States of America

²Department of Chemistry and Chemical Biology, Harvard University, 12 Oxford Street, Cambridge, Massachusetts 02138, United States of America

The library of redox-active organics that are potential candidates for electrochemical energy storage in flow batteries is exceedingly vast, necessitating high-throughput characterization of molecular lifetimes. Demonstrated extremely stable chemistries require accurate yet rapid cell cycling tests, a demand often frustrated by time-denominated capacity fade mechanisms. We have developed a high-throughput setup for elevated temperature cycling of redox flow batteries, providing a new dimension in characterization parameter space to explore. We utilize it to evaluate capacity fade rates of aqueous redox-active organic molecules, as functions of temperature. We demonstrate Arrhenius-like behavior in the temporal capacity fade rates of multiple flow battery electrolytes, permitting extrapolation to lower operating temperatures. Collectively, these results highlight the importance of accelerated decomposition protocols to expedite the screening process of candidate molecules for long lifetime flow batteries.

© 2024 The Author(s). Published on behalf of The Electrochemical Society by IOP Publishing Limited. This is an open access article distributed under the terms of the Creative Commons Attribution 4.0 License (CC BY, <http://creativecommons.org/licenses/by/4.0/>), which permits unrestricted reuse of the work in any medium, provided the original work is properly cited. [DOI: 10.1149/1945-7111/ad3855]



Manuscript submitted February 2, 2024; revised manuscript received February 26, 2024. Published April 4, 2024.

Supplementary material for this article is available [online](#)

Redox flow batteries (RFBs) comprise multiple classes of novel, as well as commercially demonstrated, energy storage electrolyte chemistries. By employing redox-active species dissolved in electrolytes pumped from external tanks into electrochemical stacks, RFBs allow for full decoupling of energy and power.¹ Currently, there is a growing interest in next-generation chemistries that could leapfrog incumbent vanadium-based electrolytes by harnessing Earth-abundant elements that are not limited by mining constraints, or hindered by uneconomic extraction.² One promising class of chemistries includes redox-active organic molecules (RAOMs) dissolved in aqueous supporting electrolytes, taking advantage of the cheapest and most abundant solvent on Earth. A multitude of redox-active molecular cores continue to be explored, with essentially infinite RAOM candidate permutations theoretically capable of being derived via synthetic chemistry.³

At long discharge durations, where RFBs are most primed for penetration into the electrical grid,⁴ the cost per kWh of aqueous organic (AORFB) systems is dominated by the cost of the electrolyte—itsself dominated by the cost of the RAOM, in comparison to the water and supporting salt.^{5–9} While there has been much focus on increasing the energy density of RFB systems via synthetic tuning of chemistries to increase solubility^{10–14} and cell voltage,^{15–18} academic pursuits typically do not examine the RFB system as a whole—the improvement of one figure of merit may come at the expense of another. Much of the concern regarding the lower volumetric energy density of RFBs, in comparison to Li-ion batteries, is somewhat unfounded for stationary energy storage systems i.e., concern for areal footprint of RFB systems may be overstated.¹⁹ One expected trade-off is increased solubility contributing to increased electrolyte viscosity, thus leading to increased pumping requirements and mass-transport limitations.^{20,21} Additionally, significant reductions in RAOM costs are still required before the cost of larger tanks (due to lower active species concentrations) becomes a considerable contribution to the total system cost.^{8,22} RAOM cost is not only an upfront capital expense for electrolyte material, but also can include the net present value (NPV) of the future costs of electrolyte replacement if the redox-active is not infinitely stable.^{7,23} This NPV increases with the temporal capacity fade rate of the

RAOM, and thus the lifetime of molecules can dictate the overall cost of an electrolyte for decadal long duration energy storage projects. Accurate measurement of capacity fade rates is paramount to NPV cost analysis, but minimizing the required time it takes to obtain such measurements is equally important when screening vast amounts of potential AORFB candidates.

Even when employing high-precision coulometry to cycle lab-scale RFBs, it appears that extremely stable aqueous RAOMs already approach the limits of precision for quantifying temporal capacity fade rates in lab-scale flow systems.²⁴ Rather than developing higher-precision instrumentation for the detection of very slow molecular degradation, or methods in which to decrease flow cell noise that are unlikely to translate to real-world scaled electrochemical systems, the goal of the work reported herein is to increase capacity fade rates to the level where quantification with standard battery cyclers is straightforward and capacity fade rate evaluation is expedited. Promoting rapid degradation can also enable in operando spectroscopic analysis of capacity fade mechanisms.^{25–29}

The use of temperature to accelerate lifetime testing is most promising in regard to increasing capacity fade rates, and has seen extensive use in the field of Li-ion batteries where Arrhenius-like relationships have often been observed e.g., in capacity fade,^{30–39} cell impedance,^{31,32,40,41} and SEI growth.^{30,32,33,35} However, the use of temperature to affect capacity fade in AORFBs is rather underdeveloped in the literature. Borchers et al.⁴² cycled an aqueous polymeric RFB at 60°C, but the use of constant current cycling—which results in uncontrolled state of charge (SOC) restriction^{24,43}—prevented any quantitative determination of the thermal stability of the redox-active species in an RFB. Rohland et al.⁴⁴ improved upon the elevated temperature cell by using a volumetrically unbalanced compositionally symmetric cell,⁴³ with a defined capacity limiting side (CLS) and non-capacity limiting side (NCLS), to cycle an aqueous anthraquinone derivative using constant current constant voltage cycling, at 60°C. However, by heating only one electrolyte reservoir of the RFB, they may have inadvertently installed a voltage difference between both reservoirs due to the temperature dependence of the reduction potential of a redox couple. This would introduce a cycling asymmetry to the cell open circuit voltage (OCV), but also affect kinetic and mass transport overpotentials on both sides of the cell disproportionately. This might decrease the equilibrium overpotential on the CLS to the point that its full capacity is not accessed during a potentiostatic

^zE-mail: maziz@harvard.edu

hold. It may also introduce a temperature gradient effect on species crossover. Symmetric cells with only one heated reservoir were used to cycle aqueous TEMPO-based RAOMS, however no statistical difference in temporal capacity fade rates at room temperature vs 40°C was observed.^{45,46} Quinn & Ripley et al.⁴⁷ investigated the effect of elevated temperature on the physicochemical and electrochemical properties, and RFB performance, of nonaqueous RAOMS up to 70°C. Many of the temperature effects explored in Ref. 47 are expected to apply to aqueous RAOMS as well—namely, increased temperature leading to increased ionic conductivity and decreased viscosity of the electrolyte, resulting in decreases in cell area-specific resistance (ASR) and mass transport limitations. The reduction of these overpotentials at elevated temperatures has enabled increased power densities for many RFB electrolytes.^{47–50} The thermal stability of a ferrocene co-polymer in a hybrid RFB has also been explored, with limited definitive results on the effect of temperature on RAOM stability.⁵¹ However, the effect of temperature on capacity fade rates in AORFBs has not yet been quantitatively demonstrated.

We have previously reported the development of a high-throughput setup for the cycling of redox flow batteries, which allows for the benchmarking of capacity fade rates and variations in cycling behavior of nominally identical flow cells.²⁴ As shown herein, augmentation of this system with elevated temperature cell cycling capabilities allows for increased testing throughput of AORFBs. We demonstrate quantitative results for accelerated lifetime testing of multiple previously published AORFB molecules via elevated temperature cycling of nominally identical volumetrically unbalanced compositionally symmetric cells. Results from over 30 elevated temperature symmetric cells are reported, along with Arrhenius relationships for temporal capacity fade rates and cell area-specific resistance in AORFBs.

Experimental

Electrolyte preparation.—Reagents used to prepare posolyte and negolyte solutions were purchased from Sigma-Aldrich and used with no further purification: potassium hydroxide, potassium ferrocyanide trihydrate, 2,6-dihydroxyanthraquinone (2,6-DHAQ⁴⁹) was purchased from Carbosynth (ID FD40589, >96% purity, 240.21 g mol⁻¹). ((9,10-dioxo-9,10-dihydroanthracene-2,6-diyl)bis(oxy))bis(propane-3,1-diyl)bis(phosphonic acid) (2,6-DPPEAQ,⁵² ID D5765, >90% purity, 484.33 g mol⁻¹) and 4,4'-((9,10-anthraquinone-2,6-diyl)dioxy)dibutylate (2,6-DBEAQ,⁵³ ID D5764, >95% purity, 412.39 g mol⁻¹) were purchased from TCI America. 1,8-dihydroxy-2,7-dicarboxymethyl-9,10-anthraquinone (1,8-DCDHAQ, 356.28 g mol⁻¹) was synthesized as reported in Ref. 54. Throughout the manuscript we refer to these chemicals as KOH, ferrocyanide, DHAQ, DPPEAQ, DBEAQ, and DCDHAQ, respectively. All electrolytes were prepared inside a N₂-filled glove box (Vacuum Atmospheres Company) with <5 ppm of oxygen, using deoxygenated deionized water that had already equilibrated with the glove box atmosphere over multiple months. Negolytes were prepared in 0.1 M concentrations of the redox-active species, with a final solution pH of 14. The set of cells for each experiment contained a respective anthraquinone negolyte chemistry at 50% SOC prepared in a single batch i.e., a large volume of negolyte was initially charged (reduced) in a single full cell against a ferrocyanide posolyte at pH 14, and then mixed with an equal volume of the initial discharged (oxidized) negolyte to form a 50% SOC electrolyte. The large volume of electrolyte was then divided across all cells in a given set to make a 5.0 ml CLS and a 10.0 ml NCLS for each cell.

Cell assembly.—All volumetrically unbalanced compositionally symmetric flow cell cycling tests were carried out with cell hardware from Fuel Cell Technologies Inc. (Albuquerque, NM), assembled into a zero-gap flow cell configuration, as described in a previous report.⁴⁹ Pyrosealed POCO graphite flow plates (9 in²) with

interdigitated flow patterns were used for both electrodes. Each electrode comprised a 5 cm² geometric surface area covered by a stack of two sheets of Sigracet GDL 39AA porous carbon paper (Fuel Cell Store) that had been pretreated by baking in air at 400°C for 24 h. The outer portion of the space between the electrodes was gasketed using Viton (PVDF) sheets (15 mils) with the area over the electrodes cut out. For all cell tests, a sheet of Nafion 117 (Ion Power Inc.) served as the ion-selective membrane between the carbon electrodes. All membranes were presoaked in 1 M KOH for two days to ion exchange the counter ions from protons to potassium ions. The torque applied during cell assembly was 60 lb-in (6.78 N·m) on each of eight 3/8"-24 bolts, thus the load applied per bolt was approximately 800 lbs. Electrolytes were fed into the cells through fluorinated ethylene propylene (FEP) tubing (each ~10 inches long) at a rate of 60 ml min⁻¹, controlled by KNF diaphragm liquid pumps (FF 12 DCB-4).

Elevated temperature cell setup.—Cells were cycled in a glove box configured for high-throughput RFB testing, previously described in Ref. 24. A Novonix battery cycler equipped with a DC-offset unit was used for all cell cycling. The temperature of the glove box atmosphere was recorded with an Arduino Uno Rev3 microcontroller equipped with DHT22 temperature sensors. An Arduino-based board controlled individual cell temperatures via PID loop of a pair of cartridge heaters per cell (4877k133, McMaster-Carr), inserted into cell end-plates, with feedback input from a K-type thermocouple (39095K96, McMaster-Carr). This setup is controlled via Python GUI, adding real-time temperature control ex situ from the glove box, complementing the previously described high-throughput system. A temperature-controlled cell is shown in Fig. S1.

Electrochemical cycling protocols.—CLS and NCLS electrolytes were pumped through cells held at the respective temperature for roughly three hours before electrochemical cycling commenced. This ensured proper wetting and equilibration of cell components, as well as providing ample time for stabilization of the glove box atmosphere temperature which increases somewhat when cells are heated. The CLS of each cell was first reduced (charged), thus the first charge half-cycle capacity is roughly half of the total capacity (i.e., the CLS is reduced from 50% to 100% SOC) and the first oxidation (discharge) half-cycle capacity is ideally the total capacity (i.e., the CLS is oxidized from 100% to 0% SOC). All cells were driven with constant voltage cycling of ±0.2 V (square wave in voltage with amplitude 0.2 V) with current cutoffs of 1 mA cm⁻² (geometric area). Electrochemical Impedance Spectroscopy (EIS) was performed with a Gamry Interface 1010B located inside the glove box, with four-point cell connections. EIS was performed at open circuit voltage with a 10 mV amplitude AC potential at frequencies ranging from 20 kHz to 10 Hz. The high-frequency intercept of the real axis of a Nyquist plot is reported as the cell ohmic resistance. Pre-electrochemical-cycling heated cell EIS measurements were obtained with both CLS and NCLS at 50% SOC.

Ex situ electrochemistry.—Cyclic and linear sweep voltammetry of 5 mM solutions of anthraquinones in 1 M KOH were performed in a three-electrode setup in a glass electrochemical cell with a water jacket for temperature control (Pine, RRP310). The counter electrode was a graphite rod (Electron Microscopy Sciences, 70230), the reference electrode was saturated mercury/mercurous sulfate (CH Instruments, CHI151, 0.640 V vs SHE), and the working electrode was glassy carbon (Pine, AFE5T050GCPK) mounted to a rotating shaft with controllable speed (Pine, AFMSRCE). The reference electrode was isolated using a salt bridge (Pine, AKTUBE1420), so that the reference electrode remained at room temperature while the working and counter electrodes were immersed in temperature-controlled electrolyte in the jacketed cell. The temperature-controlled setup is shown in Fig. S19. Before

temperature-controlled experiments, the temperature of the jacketed electrochemical cell and the temperature of the electrolyte contacting the reference electrode were both confirmed with a digital thermometer. Electrodes were connected to a Gamry Reference 3000 potentiostat. All voltammetry was performed at a sweep rate of 50 mV s^{-1} . For each voltammetry experiment of anthraquinones reported here, blank correction was performed by subtracting the equivalent voltammogram measured on the blank solution (1 M KOH) at the same temperature and working electrode rotation rate. Cyclic voltammetry with porous electrodes (Sigracet GDL 39AA and Avcarb HCBA 1186) as the working electrode was performed in a setup that was otherwise the same as the experiments with anthraquinones and glassy carbon. All voltammetry reported here was corrected for uncompensated resistance.

Results

Elevated temperature cell cycling.—The high-throughput cell cycling setup allows for testing of multiple cells initiated with the same starting batch of electrolyte. Temperature control now enables investigation of accelerated lifetime testing to facilitate enhanced screening of RAOs. Four AORFB negolytes demonstrating a range of temporal capacity fade rates were chosen for these experiments. Room temperature stability of 0.1 M active species negolytes at pH 14, acquired via potentiostatic cycling of volumetrically unbalanced compositionally symmetric cells, has been previously reported²⁴ by our group: DHAQ, $4.6 \pm 0.5\% \text{ day}^{-1}$; DPPEAQ, $0.07 \pm 0.02\% \text{ day}^{-1}$; DBEAQ, $0.03 \pm 0.01\% \text{ day}^{-1}$. A pH 14 full cell with 0.2 M DCDHAQ as negolyte demonstrated a temporal capacity fade rate of $0.09\% \text{ day}^{-1}$ at room temperature.⁵⁴ These four negolytes exhibit capacity fade rates spanning two orders of magnitude, and thus provide an appropriate starting point for exploration of the effects of elevated temperature cycling of aqueous RAOs.

We first examined the effect of temperature on cell cycling stability of eight nominally identical 0.1 M DCDHAQ pH 14 symmetric cells, cycled simultaneously in the high-throughput system. Each cell was held at a different temperature. In Fig. 1a we plot the temporal dependence of the discharge capacity normalized by the first discharge half-cycle capacity of each respective cell. An increase in capacity fade rate with increasing temperature is readily apparent. In Fig. S2 we include the non-normalized temporal- and cycle-denominated discharge capacity, and coulombic efficiency (CE). In Fig. 1b we plot the instantaneous capacity fade rate (slope of the natural log of discharge half-cycle capacity vs time) of the cells shown in Fig. 1a, as a function of temperature. The fade rate of $0.097 \pm 0.003\% \text{ day}^{-1}$ exhibited by the 30°C cell is in close agreement with the previous literature report at room temperature.⁵⁴ The temporal capacity fade data in Fig. 1b was then transformed to an Arrhenius plot, as seen in Fig. 1c. From the slope of this plot an activation energy of $87 \pm 5 \text{ kJ mol}^{-1}$ was determined.

We emphasize that this value should be considered an *apparent* activation energy because an electrochemical cell cycling experiment is not necessarily a unidirectional decomposition reaction, such as the process of heating an oxidized (or reduced) electrolyte and measuring degradation over time, sans electrochemistry, as has been done for previously reported RAOs.⁵³ During charge/discharge cycling of an RAO in an RFB, the duration that a molecule spends in the reduced or oxidized state is a function of the user-selected electrochemical cycling protocol. The decay mechanism(s), and the associated reaction rate(s) and order(s) that the given oxidation state (s) of the molecule can experience, along with the temporal rate in which electrolyte SOC changes in an RFB, are coupled cycle- and/or time-dependent processes. Zero-dimensional modelling of AORFBs^{55,56} has previously shown that temporal capacity fade rates of molecules that exhibit certain degradation mechanisms can vary depending on the electrochemical cycling protocol used. Cycling-protocol-dependent capacity fade rates have also recently

been demonstrated experimentally.²⁴ Therefore, the activation energy measured from high-throughput elevated temperature cell cycling is likely dependent on the specific electrolyte conditions and electrochemical cycling protocol used. Nonetheless, the indication of an Arrhenius-like dependence of the instantaneous capacity fade rate of DCDHAQ seen in Fig. 1c provides some amount of confidence in the extrapolation of fade rates to lower operating temperatures. By cycling RAOs at elevated temperatures, degradation is accelerated and the required cycling time is decreased, enabling high-throughput battery lifetime characterization of novel chemistries.

We next performed similar elevated temperature cycling of the more stable DPPEAQ molecule.⁵² Eight nominally identical 0.1 M DPPEAQ pH 14 symmetric cells were cycled potentiostatically ($\pm 0.2 \text{ V}$) in the high-throughput setup, with each cell held at a different temperature. We plot the temporal dependence of normalized discharge capacity of each DPPEAQ symmetric cell in Fig. 2a. Note that, due to the increased stability of DPPEAQ compared to DCDHAQ, the ordinate range in Fig. 2a represents a maximum of 1% total capacity loss, leading to the appearance of increased noise in capacity data when compared to Fig. 1a. In Fig. 2b the instantaneous capacity fade rate of the DPPEAQ symmetric cells is shown as a function of temperature. Two separate capacity fade regions are revealed, with an apparent transition near 55°C . The nearly constant temporal capacity fade rate exhibited by cells held at 50°C or below may indicate that a separate (or additional) degradation mechanism is promoted at higher temperatures, leading to distinct regions of temperature-dependent behavior seen in the Arrhenius plot of Fig. 2c. It may alternatively indicate that the differences in capacity fade rates at the lower temperatures are too slight to be detected within the precision of the cycling experiment. An investigation of the (electro)chemical decay mechanism(s) resulting in the observed capacity fade rate trends is beyond the scope of this work.

Elevated temperature symmetric cell cycling was also performed for 0.1 M DBEAQ pH 14 electrolytes (Fig. S4) and 0.1 M DHAQ pH 14 electrolytes (Fig. S6), with determined Arrhenius parameters for all negolyte chemistries reported in Table I. For DHAQ electrolytes, the maximum cell temperature tested was 50°C due to the high temporal capacity fade rate already exhibited at room temperature. Furthermore, above 30°C DHAQ electrolytes displayed telltale signs of the hydrogen evolution reaction (HER) which complicated cell cycling and warranted the use of higher current cutoffs (see further discussion in Fig. S7). Post mortem ^1H NMR analysis of oxidized electrolytes, taken after five days of electrochemical cycling, was performed for aliquots from the CLS of elevated-temperature-cycled DBEAQ and DHAQ symmetric cells. No new peaks attributable to degradation products were observed in the ^1H NMR spectra of DBEAQ electrolytes (see Figs. S8&S9), even though capacity fade was measured coulometrically in Fig. S4. This result highlights the sensitivity of coulometry compared to chemical analysis methods for rapid online detection of extremely low capacity fade rates in AORFBs. In the case of cycled DHAQ electrolytes, multiple new peaks can be seen in the ^1H NMR spectra (see Figs. S10&S11) even for electrolytes held at 30°C , consistent with the body of work characterizing fast chemical and electrochemical degradation of alkaline DHAQ electrolytes at room temperature.^{24,26–28,43,57} Finally, we note that the existence of different activation energies and Arrhenius pre-factors for temporal capacity fade, demonstrated by the RAOs shown herein, implies that the selection of an RAO based on stability is a temperature-dependent decision. As an example, our cell cycling results suggest that below 50°C DPPEAQ may be more stable than DBEAQ, whereas above that temperature, DBEAQ is more stable.

Temperature also affects overall cell ASR, which is often dominated by the ion-exchange membrane contribution—especially in alkaline conditions when employing a cation-exchange membrane. EIS measurements were performed on elevated temperature symmetric cells when both the CLS and NCLS were at 50% SOC

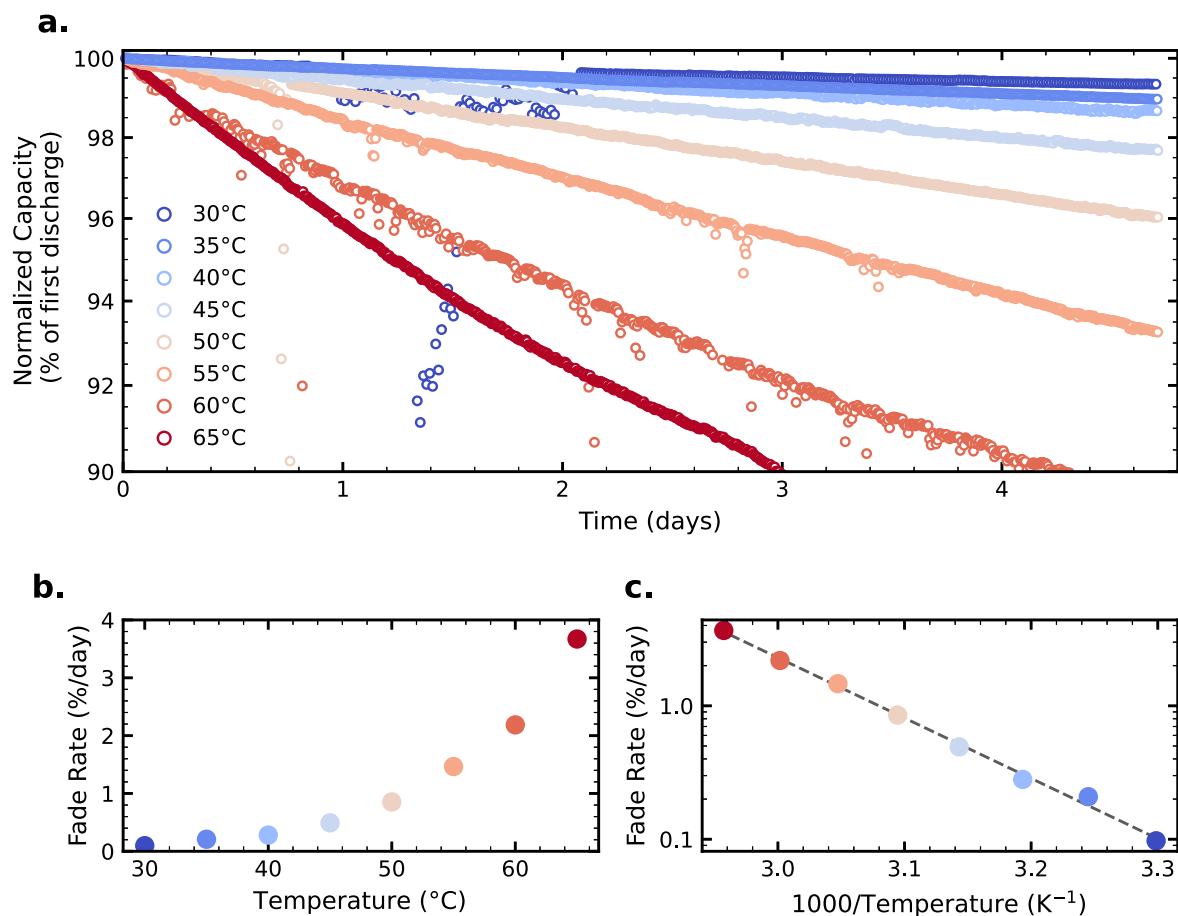


Figure 1. CV cycling (± 0.2 V) of 0.1 M DCDHAQ pH 14 symmetric cells (5.0 ml CLS vs 10.0 ml NCLS) heated at various temperatures. (a) Semi-log plot of temporal discharge capacity normalized by the first discharge capacity; (b) instantaneous capacity fade rates as functions of temperature; and (c) Arrhenius plot with dashed line of best fit.

i.e., 0 V OCV. In Fig. 3a we plot the cell ohmic ASR, determined from the high-frequency intercept of the real part of the impedance axis of a Nyquist plot, for the 0.1 M DPPEAQ pH 14 cells shown in Fig. 2. Nyquist plots from which these data are derived are shown in Fig. S12. The Arrhenius-like dependence of cell resistance contributions has been demonstrated in Li-ion batteries,^{31,32,40,41} fuel cells,^{58,59} and flow batteries⁶⁰. AORFBs are no exception—an Arrhenius dependence of cell ohmic ASR is seen in Fig. 3 for the 0.1 M DPPEAQ pH 14 cells, with fitted Arrhenius parameters reported in Table I. Corresponding elevated temperature cell ohmic ASR comparisons were obtained for DCDHAQ (Fig. S13), DBEAQ (Fig. S14), and DHAQ (Fig. S15). All symmetric cells in this work employ a Nafion 117 membrane at pH 14 KOH conditions and on average display an activation energy of conduction of -33 ± 2 kJ mol⁻¹ and Arrhenius pre-factor of 2×10^{-5} Ω cm². The good agreement across negolyte chemistries suggests that at an active species concentration of 0.1 M and pH 14 conditions, cell ASR is dominated by the Nafion 117 membrane rather than electrolyte conductivity. While the Arrhenius parameters shown in Table I provide a way to quickly estimate cell ASR at a given temperature when utilizing a cell at the same electrolyte and membrane conditions reported here, future work should explore the effects of electrolyte composition, membrane thickness, and membrane composition on both the activation energy of conduction and the Arrhenius pre-factor. Electrolyte mass fractions in hydrated membranes have been shown to affect how ion concentration dictates membrane conductivity,⁶¹ and temperature provides a new dimension in which to explore these effects and their relationship to RFB system metrics such as volumetric energy density and areal power density.

As cell and electrolyte temperatures increase (resulting in decreased cell ohmic ASR), potentiostatic cycle durations tend to decrease due to higher achievable cell currents. With the cell temperature control employed in this work, we no longer see a distinct inverse correlation between variations in glove box atmosphere temperature and potentiostatic half-cycle duration, previously observed for uncontrolled-temperature cells in²⁴. Discharge half-cycle duration of select elevated temperature 0.1 M DPPEAQ pH 14 symmetric cells (from Fig. 2) are shown in Fig. S16, demonstrating increased half-cycle durations at lower cell temperatures. Shorter half-cycles enabled by higher currents is visualized in Fig. S17 where we plot the maximum absolute current density during charging and discharging half-cycles for select 0.1 M DPPEAQ pH 14 symmetric cells of Fig. 2. We observe an increase in the maximum absolute current density (of half-cycles) with temperature, as well as consistent maximum absolute current density values for the duration of cycling. Surprisingly, a similar analysis of the 0.1 M DHAQ pH 14 symmetric cells (cell data in Fig. S6) also shows consistent maximum absolute current density values over the duration of cycling even though significant apparent capacity fade has occurred, as seen in Fig. S18. After five days of cycling, the 40°C DPPEAQ cell of Fig. S17 displayed 0.2% total capacity loss whereas the 40°C DHAQ cell of Fig. S18 experienced 68% capacity loss, according to coulometry. Yet both cells display consistent maximum absolute current densities for both charge and discharge half-cycles throughout the duration of cycling. This is likely an indication of the lack of mass transport limitations at the beginning of half-cycles.

As a final consideration, a logical next step for RAOB characterization via elevated temperature cycling after performing

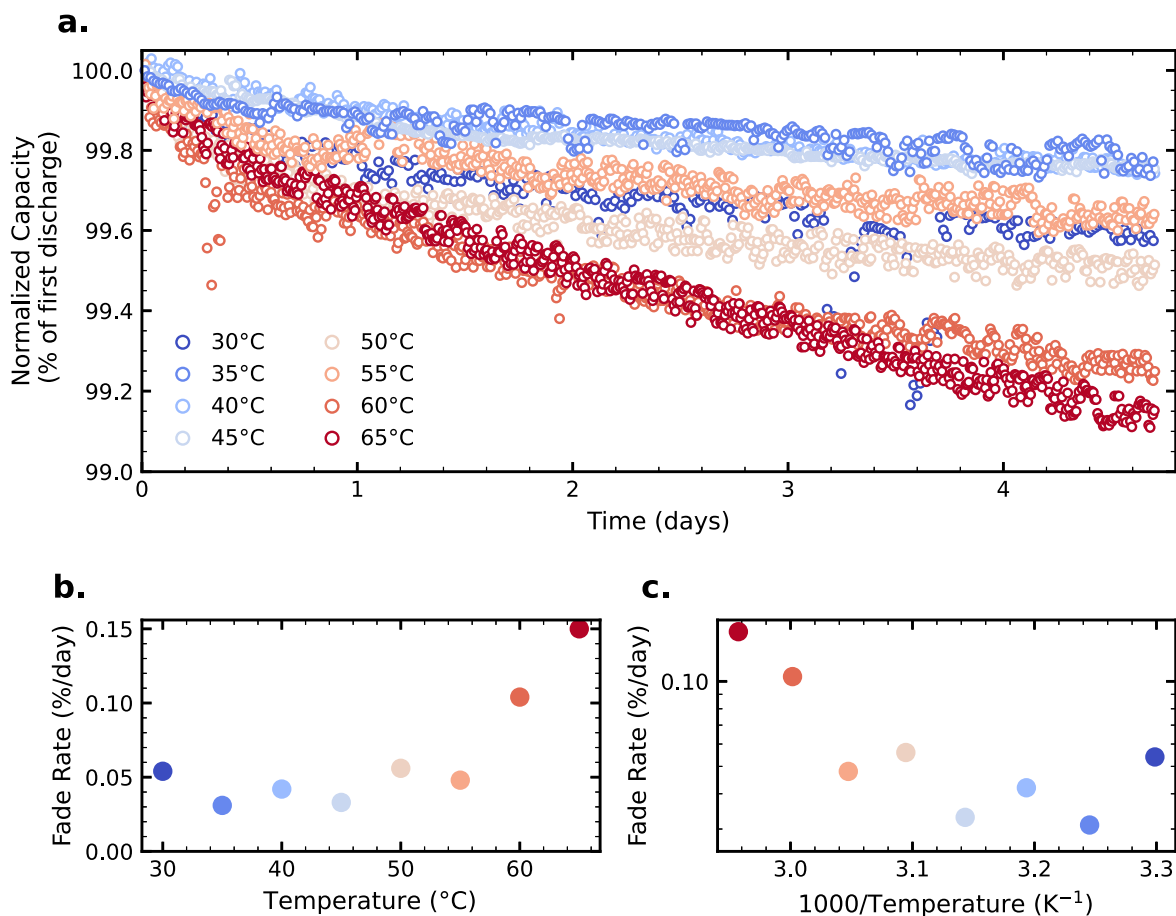


Figure 2. CV cycling (± 0.2 V) of 0.1 M DPPEAQ pH 14 symmetric cells (5.0 ml CLS vs 10.0 ml NCLS) heated at various temperatures. (a) Semi-log plot of temporal discharge capacity normalized by the first discharge capacity; (b) instantaneous capacity fade rates as functions of temperature; and (c) Arrhenius plot.

Table I. Arrhenius parameters for temporal capacity fade and cell ohmic ASR determined from elevated temperature symmetric cell cycling.

Molecule	E_a^f (kJ mol ⁻¹) ^a	f_0 (% day ⁻¹) ^b	E_a^R (kJ mol ⁻¹) ^c	R_0 (Ω cm ²) ^d
DCDHAQ (Fig. 1)	87 \pm 5	8.6×10^{13}	-33 \pm 3	1.1×10^{-5}
DPPEAQ (Fig. 2)	2 \pm 51 ^e 105 \pm 260 ^f	8.3×10^{-2} 3.0 $\times 10^{15}$	-31 \pm 2	2.5×10^{-5}
DBEAQ (Fig. S4)	34 \pm 9	2.1×10^4	-32 \pm 1	1.7×10^{-5}
DHAQ (Fig. S6)	39 \pm 4 ^g	5.1×10^7	-35 \pm 4	4.6×10^{-6}

Notes.a) Activation energy for temporal capacity fade; b) Arrhenius pre-factor of temporal capacity fade; c) Activation energy of conduction; d) Arrhenius pre-factor of conduction; e) At 50°C and below; f) Above 50°C; g) Based on two 30°C cells and two 40°C cells;

symmetric cell tests would be to advance to full cells. In alkaline conditions, long-term demonstrations of AORFBs have typically employed ferri-/ferrocyanide posolytes.^{3,62} Unfortunately, when cycling full cells at 55°C with pH 14 ferri-/ferrocyanide posolytes, we have detected free cyanide and observed rust-colored precipitates in reservoirs, indicative of the previously reported thermal degradation of alkaline ferricyanide electrolytes at elevated temperatures.⁶³ Full cells with pH 14 ferri-/ferrocyanide posolytes held at 35°C displayed no such issues. Without chemical processing or rebalancing methods, this may require temperature control in the electrochemical stacks of deployed AORFB systems. Additionally, the effect of temperature on RAOM crossover through the ion-exchange membrane—and the requirement for recovery strategies that may ensue—cannot be neglected in full cells.^{61,64} Thermal stability of membranes (and other cell components) must also be confirmed, if cells are to be run at elevated temperatures.

Ex situ electrochemistry.—We next explored the effect of temperature on the electrochemical half-reactions of interest, via ex situ techniques such as cyclic voltammetry (CV) and rotating disk electrode (RDE). CVs of 5 mM DPPEAQ pH 14 electrolytes at various temperatures are seen in Fig. 4. Increased temperature results in a subtle negative shift of the potentials at peak oxidation and reduction currents, and thus a negative shift of half-wave potentials ($E_{1/2}$) is observed. Under dilute solution conditions and assumption of similar diffusion coefficients for oxidized and reduced species, $E_{1/2} \approx E^\circ$, where E° is the formal reduction potential. We obtain $E_{1/2}$, and thereby obtain E° , values from the CVs at each temperature in Fig. 4 to calculate the temperature derivative of the formal reduction potential ($\frac{dE^\circ}{dT}$), often referred to as the formal temperature coefficient. The determined temperature derivative for DPPEAQ is -0.3 mV K⁻¹, similar in magnitude to literature values for inorganic redox couples used in aqueous RFBs.^{65–67}

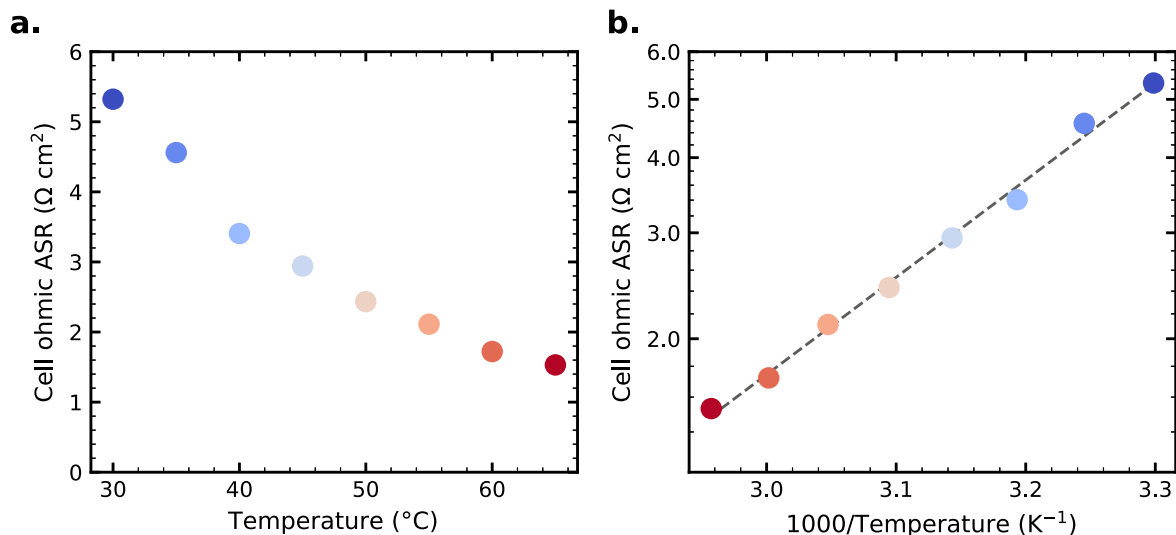


Figure 3. Ohmic ASR of 0.1 M DPPEAQ pH 14 symmetric cells shown in Fig. 2, (a) as a function of cell temperature; and (b) Arrhenius plot with dashed line of best fit. Regression parameters are reported in Table I.

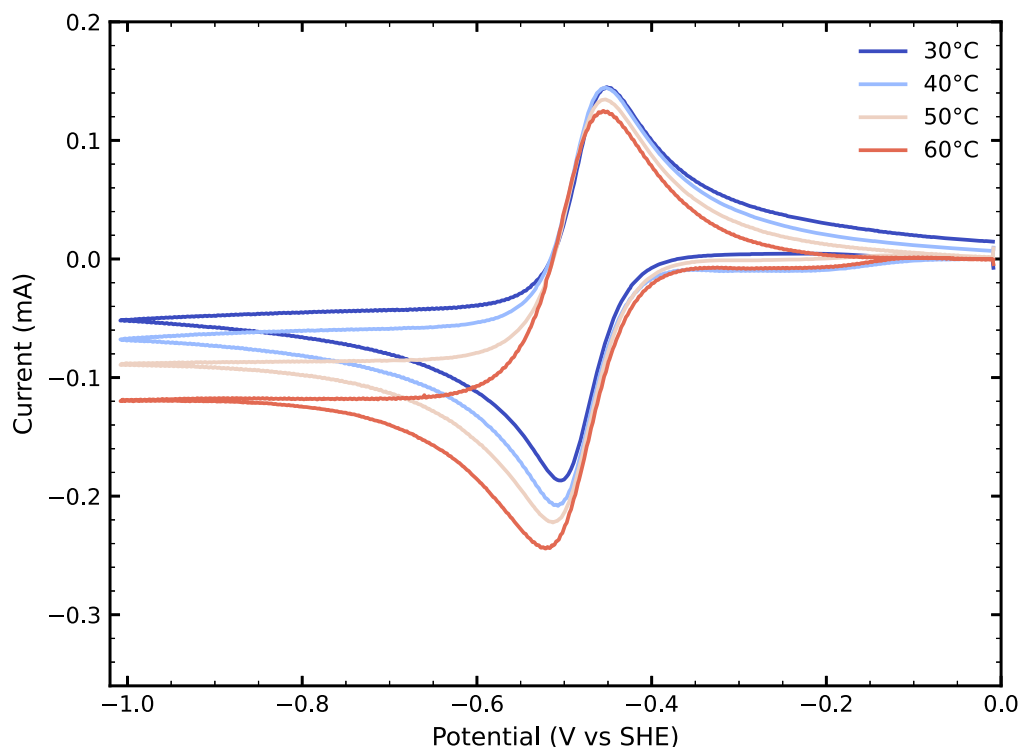


Figure 4. Cyclic voltammograms of 5 mM DPPEAQ pH 14 at a sweep rate of 50 mV s^{-1} .

Elevated temperature CVs were also acquired for DCDHAQ (Fig. S20), DBEAQ (Fig. S21), and DHAQ (Fig. S22). All anthraquinone negolytes investigated herein exhibit negative formal reduction potential temperature derivatives, and thus negative standard formal entropy changes of reduction,^{65,68,69} and are reported in Table S1. From an electrochemical system design perspective, pairing a negolyte exhibiting a negative (positive) formal temperature coefficient with a posolyte exhibiting a positive (negative) formal temperature coefficient would provide an expanded cell voltage with increased (decreased) temperature. If both formal temperature coefficients are of the same sign, there may be little to no change in cell voltage with temperature. Judicious selection of negolyte and posolyte chemistries may also be beneficial for non-isothermal cycling of RFBs i.e., charging and discharging

the battery at different temperatures. Lowering the charging voltage and raising the discharging voltage via changes in OCV (through formal temperature coefficients), and possibly through changes in overpotentials (which will decrease with temperature), could increase voltage efficiency. Improved voltage efficiency under non-isothermal cycling conditions has been demonstrated for vanadium-based RFBs,⁶⁶ Li-ion batteries,⁷⁰ and thermally regenerative electrochemical cycles.^{67,71}

Diffusion coefficients, electrochemical rate constants, and charge transfer coefficients were determined by RDE for 5 mM anthraquinone negolytes at pH 14. Levich, Koutecký–Levich, and Tafel analyses were performed for each negolyte at various temperatures, and are described in the supporting information. A comparison of select rotation speed RDE voltammograms of DPPEAQ, taken at

four temperatures, is seen in Fig. 5a. Increased temperatures result in increased absolute currents in the mass transport limited regime, indicative of an increasing diffusion coefficient. The temperature dependence of diffusion is readily apparent in the Arrhenius plot of Fig. 5b. A similar analysis is performed in Fig. 5c for electrochemical rate constants obtained from Tafel analysis at multiple temperatures, and once again an Arrhenius relationship is observed. These results demonstrate that increased temperature can reduce overpotentials associated with mass transport and activation limitations by increasing RAO diffusion coefficients and electrochemical rate constants, respectively. From the Arrhenius analysis of Fig. 5b& 5c activation energies of diffusion and electrochemical rate constant are calculated, reported in Table S2, along with Arrhenius pre-factors. We refer the reader to comparisons of elevated temperature RDE for DCDHAQ (Fig. S27), DBEAQ (Fig. S36), and DHAQ (Fig. S41).

The following general trends are noted: 1) DHAQ exhibits a larger diffusion coefficient at all temperatures compared to other negolytes, which could be explained in part by the lack of large functional groups attached to the anthraquinone core, compared to DCDHAQ/DPPEAQ/DBEAQ. Both size and charge effects can influence diffusion coefficients of RAOs,⁷² and the molecules studied herein vary in charge number when deprotonated in strongly alkaline conditions e.g., -2 for DHAQ, -4 for DPPEAQ; 2) minimal change in charge transfer coefficient with increased temperature is seen for all species; 3) each molecule exhibits similar activation energies of diffusion and electrochemical rate constant, but orders of magnitude differences are seen in the respective Arrhenius pre-factors. Further studies in less-alkaline pH regimes where these RAOs undergo proton-coupled electron transfer could yield other

useful information such as reorganization energies, double layer effects on standard rate constants, and solvent effects.^{73–75}

An additional consideration for elevated temperature cycling of RAOs in aqueous RFBs is the temperature-dependent electrochemical stability of water. Extended windows of ideal polarizability (beyond thermodynamic water splitting limits) have been demonstrated for many aqueous systems via kinetic stabilization by judicious selection of electrolyte/electrode composition.^{17,76,77} To the best of our knowledge, however, elevated temperature aqueous stability windows on RFB porous electrode materials have not been previously demonstrated in alkaline electrolytes, pertinent to the RAOs studied in this work. We examined the temperature-dependent aqueous stability window, employing commercial porous carbon electrodes used in RFB systems. Linear sweep voltammetry was performed with glassy carbon, carbon cloth, and carbon paper working electrodes in 1 M KOH supporting electrolyte, shown in Fig. 6. Absolute faradaic currents, at a given onset potential, are seen to increase with temperature on each electrode material, which we assume to be dominated by HER and oxygen evolution reaction (OER) at more negative and more positive potentials, respectively. This demonstrates that even at elevated temperatures, the aqueous stability window within which candidate RAOs could be selected for AORFB systems is much larger than the (often concerningly mentioned) thermodynamic stability window, although all electrodes demonstrate a decreased polarization window with increasing temperature. Gaseous products from parasitic HER and OER currents can still be managed in aqueous batteries via gas-consumption devices^{17,78} but the safety of such systems at elevated temperatures must be studied.⁷⁹ As negolyte (posolyte) chemistries are developed with further negative (positive) reduction potentials,

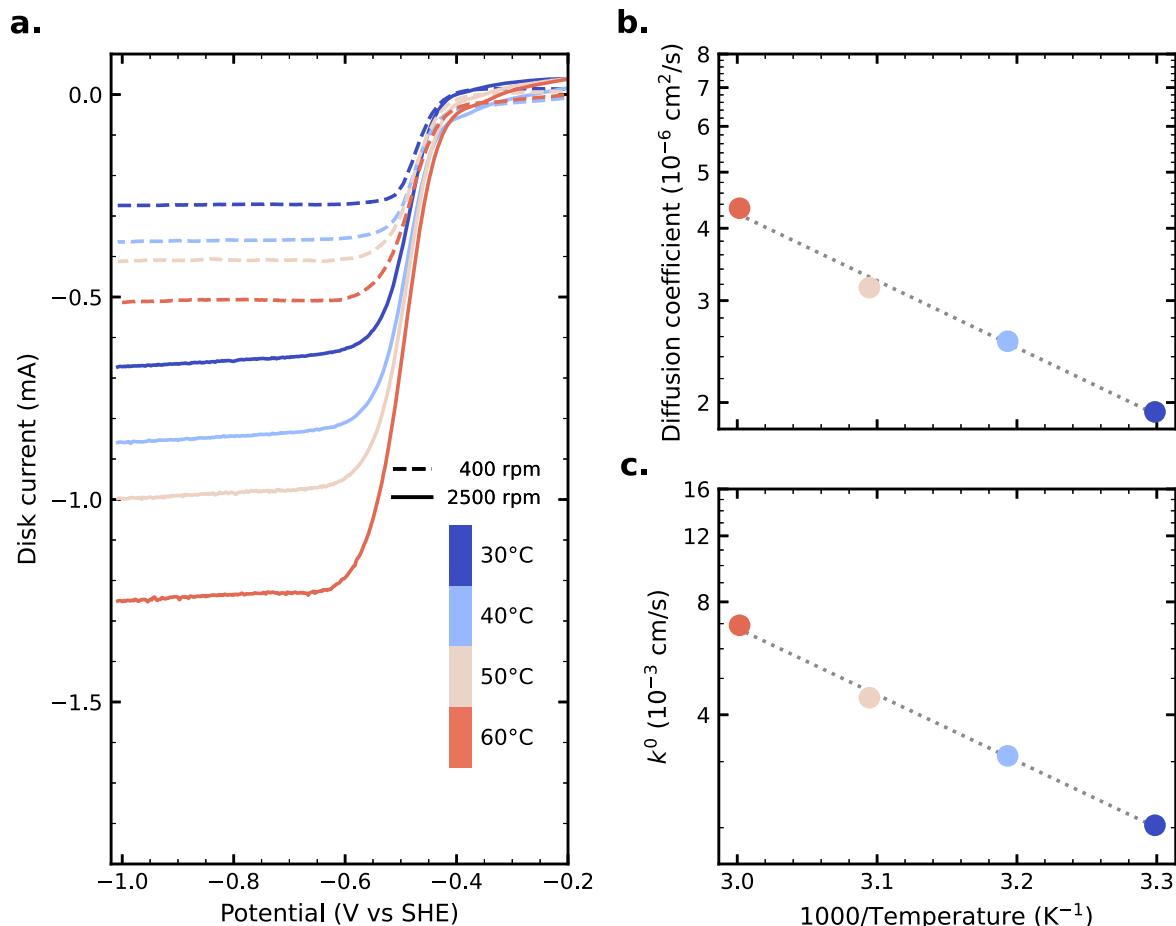


Figure 5. Comparison of RDE analysis of 5 mM DPPEAQ pH 14 with select linear sweep voltammograms shown in (a). Arrhenius plots of (b) diffusion coefficients obtained from the respective Levich analyses, and (c) electrochemical rate constants obtained from the respective Tafel analyses, with dashed lines of best fit. See Figs. S28–S31 for comprehensive data.

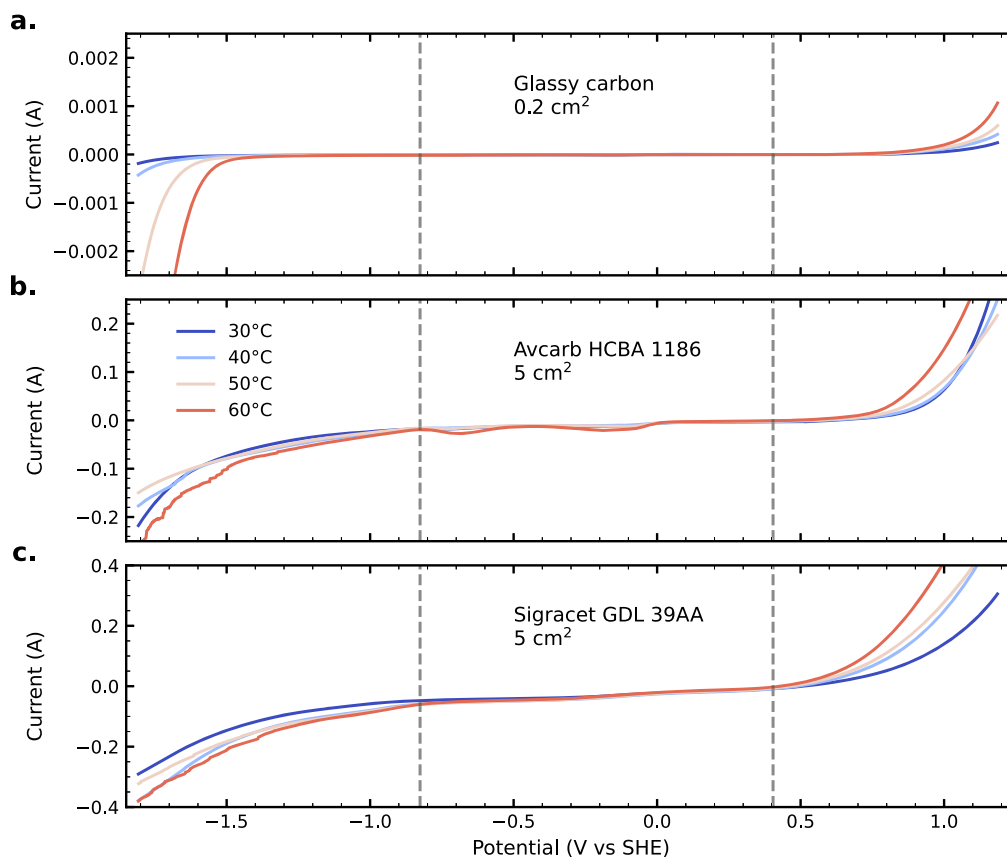


Figure 6. Linear sweep voltammograms of 1 M KOH blank electrolyte at a sweep rate of 50 mV s^{-1} , at various temperatures. The working electrode material was (a) glassy carbon; (b) Avcarb HCBA 1186 carbon cloth; and (c) Sigracet GDL 39AA carbon paper. Dashed vertical lines denote the thermodynamic water-splitting window at pH 14 and 25°C . Electrode geometric areas are listed.

parasitic homo-/heterogeneous water-splitting may become more pronounced.

As a result of the observed temperature-dependent reduction potentials, overpotentials, and solvent stability, the question of what constitutes a valid comparison of nominally identical full cells—differing only in temperature—is also raised. Identical cells held at different temperatures, even if charged and discharged at the same fixed voltages, will have different OCV values and the distribution of cell overpotential shared between negolyte and posolyte may vary. It is unclear how best to characterize AORFB full cells as a function of temperature, but it likely involves the judicious selection of electrochemical cycling protocols to enable like-for-like comparison.

Conclusions

We demonstrate elevated temperature RFB cycling of aqueous RAOMs that exhibit an Arrhenius-like dependence of temporal capacity fade rates (DCDHAQ, DBEAQ), enabling high-throughput battery lifetime characterization of flow battery chemistries via accelerated testing. However, the presence of multiple degradation mechanisms with differing Arrhenius behavior for a given RAOM may complicate lifetime prediction by simple extrapolation (possibly seen with DPPEAQ). The investigation of the Arrhenius behavior of DHAQ was frustrated by HER. Differing temperature-dependent capacity fade rate behavior amongst RAOMs also demonstrates that a more stable chemistry at one temperature may not be the most stable candidate at another.


In line with previous work, elevated temperature can increase RAOM diffusion coefficients and electrochemical rate constants, and decrease cell ohmic ASR, all of which contribute to lowering overpotential losses. Of the anthraquinone negolytes studied, all demonstrate negative temperature derivatives of formal reduction

potentials, thus indicating that a small increase in cell voltage can be achieved at elevated temperature with an appropriately chosen posolyte. Finally, diminution of the electrochemical kinetic stability window of the aqueous solvent with temperature suggests that temperature selection for an AORFB system will involve the optimization of RAOM and solvent stability, cell voltage, and overpotentials.

Acknowledgments

This research was supported in part by U.S. DOE award DE-AC05-76RL01830 through PNNL subcontract 654 799 and in part by U.S. DOE award DE-EE0009795 through subcontract QE-SC-2022-02 from Quino Energy. T.Y.G. was supported in part by the NSF Graduate Research Fellowship Program. The authors are indebted to Jim MacArthur of the Harvard Electronics Shop for assistance with development of temperature controllers. We are very grateful for stimulating discussions and feedback from Jordan Sosa.

ORCID

Eric M. Fell  <https://orcid.org/0000-0003-2046-1480>
 Thomas Y. George  <https://orcid.org/0000-0002-0159-8521>
 Michael J. Aziz  <https://orcid.org/0000-0001-9657-9456>

References

1. *Flow Batteries: From Fundamentals to Applications*. C. Roth, J. Noack, and M. Skyllas-Kazacos (ed.), (Wiley) (2023).
2. K. E. Rodby, R. L. Jaffe, E. A. Olivetti, and F. R. Brushett, "Materials availability and supply chain considerations for vanadium in grid-scale redox flow batteries." *Journal of Power Sources*, **560**, 232605 (2023).
3. D. G. Kwabi, Y. Ji, and M. J. Aziz, "Electrolyte lifetime in aqueous organic redox flow batteries: A critical review." *Chem. Rev.*, **120**, 6467 (2020).

4. M. S. Ziegler, J. M. Mueller, G. D. Pereira, J. Song, M. Ferrara, Y.-M. Chiang, and J. E. Trancik, "Storage requirements and costs of shaping renewable energy toward grid decarbonization." *Joule*, **3**, 2134 (2019).
5. R. M. Darling, K. G. Gallagher, J. A. Kowalski, S. Ha, and F. R. Brushett, "Pathways to low-cost electrochemical energy storage: a comparison of aqueous and nonaqueous flow batteries." *Energy & Environmental Science*, **7**, 3459 (2014).
6. R. Dmello, J. D. Milshtein, F. R. Brushett, and K. C. Smith, "Cost-driven materials selection criteria for redox flow battery electrolytes." *Journal of Power Sources*, **330**, 261 (2016).
7. F. R. Brushett, M. J. Aziz, and K. E. Rodby, "On lifetime and cost of redox-active organics for aqueous flow batteries." *ACS Energy Lett.*, **5**, 879 (2020).
8. T. D. Gregory, M. L. Perry, and P. Albertus, "Cost and price projections of synthetic active materials for redox flow batteries." *Journal of Power Sources*, **499**, 229965 (2021).
9. R. M. Darling, "Techno-economic analyses of several redox flow batteries using leveled cost of energy storage." *Current Opinion in Chemical Engineering*, **37**, 100855 (2022).
10. S. Jin, Y. Jing, D. G. Kwabi, Y. Ji, L. Tong, D. De Porcellinis, M.-A. Goulet, D. A. Pollack, R. G. Gordon, and M. J. Aziz, "A water-miscible quinone flow battery with high volumetric capacity and energy density." *ACS Energy Lett.*, **4**, 1342 (2019).
11. D. Reber, J. R. Thurston, M. Becker, and M. P. Marshak, "Stability of highly soluble ferrocyanides at neutral pH for energy-dense flow batteries." *Cell Reports Physical Science*, **4**, 101215 (2023).
12. E. F. Kerr, Z. Tang, T. Y. George, S. Jin, E. M. Fell, K. Amini, Y. Jing, M. Wu, R. G. Gordon, and M. J. Aziz, "High energy density aqueous flow battery utilizing extremely stable, branching-induced high-solubility anthraquinone near neutral pH." *ACS Energy Lett.*, **8**, 600 (2023).
13. K. Amini, E. F. Kerr, T. Y. George, A. M. Alfaraidi, Y. Jing, T. Tsukamoto, R. G. Gordon, and M. J. Aziz, "An extremely stable, highly soluble monosubstituted anthraquinone for aqueous redox flow batteries." *Adv. Funct. Mater.*, **33**, 2211338 (2023).
14. K. Peng, P. Sun, Z. Yang, and T. Xu, "A PEGylated viologen for crossover-free and high-capacity pH-Neutral aqueous organic redox flow batteries." *Batteries & Supercaps*, **6**, e202200426 (2023).
15. B. H. Robb, J. M. Farrell, and M. P. Marshak, "Chelated chromium electrolyte enabling high-voltage aqueous flow batteries." *Joule*, **3**, 2503 (2019).
16. B. H. Robb, S. E. Waters, J. D. Saraidaridis, and M. P. Marshak, "Realized potential as neutral pH flow batteries achieve high power densities." *Cell Reports Physical Science*, **3**, 101118 (2022).
17. M. L. Perry, K. E. Rodby, and F. R. Brushett, "Untapped potential: The need and opportunity for high-voltage aqueous redox flow batteries." *ACS Energy Lett.*, **7**, 659 (2022).
18. K. Amini, A. N. Shocron, M. E. Suss, and M. J. Aziz, "Pathways to high-power-density redox flow batteries." *ACS Energy Lett.*, **8**, 3526 (2023).
19. D. Reber, S. R. Jarvis, and M. P. Marshak, "Beyond energy density: flow battery design driven by safety and location." *Energy Advances*, **2**, 1357 (2023).
20. J. D. Milshtein, K. M. Tenny, J. L. Barton, J. Drake, R. M. Darling, and F. R. Brushett, "Quantifying mass transfer rates in redox flow batteries." *J. Electrochem. Soc.*, **164**, E3265 (2017).
21. J. D. Milshtein, R. M. Darling, J. Drake, M. L. Perry, and F. R. Brushett, "The critical role of supporting electrolyte selection on flow battery cost." *J. Electrochem. Soc.*, **164**, A3883 (2017).
22. P. Albertus, J. S. Manser, and S. Litzelman, "Long-duration electricity storage applications, economics, and technologies." *Joule*, **4**, 21 (2020).
23. K. E. Rodby, M. L. Perry, and F. R. Brushett, "Assessing capacity loss remediation methods for asymmetric redox flow battery chemistries using leveled cost of storage." *Journal of Power Sources*, **506**, 230085 (2021).
24. E. M. Fell and M. J. Aziz, "High-throughput electrochemical characterization of aqueous organic redox flow battery active material." *J. Electrochem. Soc.*, **170**, 100507 (2023).
25. L. Tong, Q. Chen, A. A. Wong, R. Gómez-Bombarelli, A. Aspuru-Guzik, R. G. Gordon, and M. J. Aziz, "UV-Vis spectrophotometry of quinone flow battery electrolyte for in situ monitoring and improved electrochemical modeling of potential and quinhydrone formation." *Phys. Chem. Chem. Phys.*, **19**, 31684 (2017).
26. E. W. Zhao et al., "In situ NMR metrology reveals reaction mechanisms in redox flow batteries." *Nature*, **579**, 224 (2020).
27. E. W. Zhao, E. Jönsson, R. B. Jethwa, D. Hey, D. Lyu, A. Brookfield, P. A. A. Klusener, D. Collison, and C. P. Grey, "Coupled in situ nmr and epr studies reveal the electron transfer rate and electrolyte decomposition in redox flow batteries." *J. Am. Chem. Soc.*, **143**, 1885 (2021).
28. Y. Jing et al., "In situ electrochemical recombination of decomposed redox-active species in aqueous organic flow batteries." *Nat. Chem.*, **14**, 1103 (2022).
29. S. V. Modak, W. Shen, S. Singh, D. Herrera, F. Oudeif, B. R. Goldsmith, X. Huan, and D. G. Kwabi, "Understanding capacity fade in organic redox-flow batteries by combining spectroscopy with statistical inference techniques." *Nat. Commun.*, **14**, 3602 (2023).
30. M. Broussely, S. Herreyre, P. Biensan, P. Kasztejna, K. Nechev, and R. J. Staniewicz, "Aging mechanism in Li ion cells and calendar life predictions." *Journal of Power Sources*, **97-98**, 13 (2001).
31. B. Y. Liaw, E. P. Roth, R. G. Jungst, G. Nagasubramanian, H. L. Case, and D. H. Doughty, "Correlation of Arrhenius behaviors in power and capacity fades with cell impedance and heat generation in cylindrical lithium-ion cells." *Journal of Power Sources*, **119-121**, 874 (2003).
32. S. Käbitz, J. B. Gerschler, M. Ecker, Y. Yurdagel, B. Emmermacher, D. André, T. Mitsch, and D. U. Sauer, "Cycle and calendar life study of a graphite|LiNi_{1/3}Mn_{1/3}Co_{1/3}O₂ Li-ion high energy system. Part A: Full cell characterization." *Journal of Power Sources*, **239**, 572 (2013).
33. D. A. Stevens, R. Y. Ying, R. Fathi, J. N. Reimers, J. E. Harlow, and J. R. Dahn, "Using high precision coulometry measurements to compare the degradation mechanisms of NMC/LMO and NMC-Only automotive scale pouch cells." *J. Electrochem. Soc.*, **161**, A1364 (2014).
34. T. Waldmann, M. Kasper, and M. Wohlfahrt-Mehrens, "Optimization of charging strategy by prevention of lithium deposition on anodes in high-energy lithium-ion batteries—electrochemical experiments." *Electrochimica Acta*, **178**, 525 (2015).
35. X.-G. Yang and C.-Y. Wang, "Understanding the trilemma of fast charging, energy density and cycle life of lithium-ion batteries." *Journal of Power Sources*, **402**, 489 (2018).
36. J. E. Harlow et al., "A wide range of testing results on an excellent Lithium-Ion cell chemistry to be used as benchmarks for new battery technologies." *J. Electrochem. Soc.*, **166**, A3031 (2019).
37. A. Eldesoky et al., "Impact of graphite materials on the lifetime of NMC811/Graphite pouch cells: Part II. long-term cycling, stack pressure growth, isothermal microcalorimetry, and lifetime projection." *J. Electrochem. Soc.*, **169**, 010501 (2022).
38. T. Taskovic, A. Eldesoky, W. Song, M. Bauer, and J. R. Dahn, "High temperature testing of NMC/Graphite cells for rapid cell performance screening and studies of electrolyte degradation." *J. Electrochem. Soc.*, **169**, 040538 (2022).
39. G. Kucinskis, M. Bozorgchenani, M. Feinauer, M. Kasper, M. Wohlfahrt-Mehrens, and T. Waldmann, "Arrhenius plots for Li-ion battery ageing as a function of temperature, C-rate, and ageing state—An experimental study." *Journal of Power Sources*, **549**, 232129 (2022).
40. I. Bloom et al., "An accelerated calendar and cycle life study of Li-ion cells." *Journal of Power Sources*, **101**, 238 (2001).
41. M. C. Smart, J. F. Whitacre, B. V. Ratnakumar, and K. Amine, "Electrochemical performance and kinetics of Li_{1+x}(Co_{1/3}Ni_{1/3}Mn_{1/3})_{1-x}O₂ cathodes and graphite anodes in low-temperature electrolytes." *Journal of Power Sources*, **168**, 501 (2007).
42. P. S. Borchers, M. Strumpf, C. Friebe, I. Nischang, M. D. Hager, J. Elbert, and U. S. Schubert, "Aqueous redox flow battery suitable for high temperature applications based on a tailor-made ferrocene copolymer." *Adv. Energy Mater.*, **10**, 2001825 (2020).
43. M.-A. Goulet and M. J. Aziz, "Flow battery molecular reactant stability determined by symmetric cell cycling methods." *J. Electrochem. Soc.*, **165**, A1466 (2018).
44. P. Rohland, K. Schreyer, M. D. Hager, and U. S. Schubert, "Anthraquinone-2,6-disulfamic acid: an anolyte with low decomposition rates at elevated temperatures." *RSC Adv.*, **11**, 38759 (2021).
45. O. Nolte, P. Rohland, N. Ueberschaar, M. D. Hager, and U. S. Schubert, "Stability of TMA-TEMPO-based aqueous electrolytes for redox-flow batteries." *Journal of Power Sources*, **525**, 230996 (2022).
46. P. Rohland, O. Nolte, K. Schreyer, H. Görts, M. D. Hager, and U. S. Schubert, "Structural alterations on the TEMPO scaffold and their impact on the performance as active materials for redox flow batteries." *Materials Advances*, **3**, 4278 (2022).
47. A. H. Quinn, K. M. Ripley, N. J. Matteucci, B. J. Neyhouse, C. A. O. Brown, W. P. Woltmann, and F. R. Brushett, "Elucidating the effects of temperature on nonaqueous redox flow cell cycling performance." *J. Electrochem. Soc.*, **170**, 120520 (2023).
48. K. T. Cho, P. Ridgway, A. Z. Weber, S. Haussener, V. Battaglia, and V. Srinivasan, "High performance hydrogen/bromine redox flow battery for grid-scale energy storage." *J. Electrochem. Soc.*, **159**, A1806 (2012).
49. K. Lin et al., "Alkaline quinone flow battery." *Science*, **349**, 1529 (2015).
50. C. Zhang, T. S. Zhao, Q. Xu, L. An, and G. Zhao, "Effects of operating temperature on the performance of vanadium redox flow batteries." *Applied Energy*, **155**, 349 (2015).
51. I. A. Volodin et al., "Evaluation of in situ thermal stability assessment for flow batteries and deeper investigation of the ferrocene co-polymer." *Journal of Materials Chemistry A*, **12**, 4806 (2024).
52. Y. Ji, M.-A. Goulet, D. A. Pollack, D. G. Kwabi, S. Jin, D. De Porcellinis, E. F. Kerr, R. G. Gordon, and M. J. Aziz, "A phosphate-functionalized quinone redox flow battery at near-neutral pH with record capacity retention rate." *Adv. Energy Mater.*, **9**, 1900039 (2019).
53. D. G. Kwabi et al., "Alkaline quinone flow battery with long lifetime at pH 12." *Joule*, **2**, 1894 (2018).
54. M. Wu, M. Bahari, E. M. Fell, R. G. Gordon, and M. J. Aziz, "High-performance anthraquinone with potentially low cost for aqueous redox flow batteries." *Journal of Materials Chemistry A*, **9**, 26709 (2021).
55. S. Modak and D. G. Kwabi, "A zero-dimensional model for electrochemical behavior and capacity retention in organic flow cells." *J. Electrochem. Soc.*, **168**, 080528 (2021).
56. E. M. Fell, J. A. Fell, and M. J. Aziz, "RFBzero: A python package for zero-dimensional simulation of redox flow battery cycling." *Journal of Open Source Software*, submitted, Software available at <https://pypi.org/project/rfbzero/>, version 1.0.0.post1..
57. M.-A. Goulet, L. Tong, D. A. Pollack, D. P. Tabor, S. A. Odom, A. Aspuru-Guzik, E. E. Kwan, R. G. Gordon, and M. J. Aziz, "Extending the lifetime of organic flow batteries via redox state management." *J. Am. Chem. Soc.*, **141**, 8014 (2019).
58. S. Asghari, A. Mokmeli, and M. Samavati, "Study of PEM fuel cell performance by electrochemical impedance spectroscopy." *International Journal of Hydrogen Energy*, **35**, 9283 (2010).
59. S. J. Andreasen, J. R. Vang, and S. K. Kær, "High temperature PEM fuel cell performance characterisation with CO and CO₂ using electrochemical impedance spectroscopy." *International Journal of Hydrogen Energy*, **36**, 9815 (2011).

60. D. Hoffmeyer, "Organic redox flow batteries: Active materials and reactor performance." *Ph.D. thesis*, Technical University of Denmark (2021).
61. T. Y. George, I. C. Thomas, N. O. Haya, J. P. Deneen, C. Wang, and M. J. Aziz, "Membrane-electrolyte system approach to understanding ionic conductivity and crossover in alkaline flow cells." *ACS Applied Materials & Interfaces*, **15**, 57252 (2023).
62. E. M. Fell, D. De Porcellinis, Y. Jing, V. Gutierrez-Venegas, T. Y. George, R. G. Gordon, S. Granados-Focil, and M. J. Aziz, "Long-term stability of Ferri-/Ferrocyanoide as an Electroactive component for redox flow battery applications: On the origin of apparent capacity fade." *J. Electrochem. Soc.*, **170**, 070525 (2023).
63. G. B. Adams, R. P. Hollandsworth, and B. D. Webber, (1979), Rechargeable alkaline zinc/ferricyanoide battery: Final Report for the Period 29 September 1978-28 September 1979 (Lockheed Palo Alto Research Laboratory, Lockheed Missiles & Space Co., Palo Alto, Calif.).
64. M. L. Perry, J. D. Saraidaridis, and R. M. Darling, "Crossover mitigation strategies for redox-flow batteries." *Current Opinion in Electrochemistry*, **21**, 311 (2020).
65. A. J. deBethune, T. S. Licht, and N. Swendeman, "The temperature coefficients of electrode potentials: The isothermal and thermal coefficients—The standard ionic entropy of electrochemical transport of the hydrogen Ion." *J. Electrochem. Soc.*, **106**, 616 (1959).
66. N. S. Hudak, "Practical thermodynamic quantities for aqueous vanadium- and iron-based flow batteries." *Journal of Power Sources*, **269**, 962 (2014).
67. J. Bleeker, S. Reichert, J. Veerman, and D. A. Vermaas, "Thermo-electrochemical redox flow cycle for continuous conversion of low-grade waste heat to power." *Sci. Rep.*, **12**, 7993 (2022).
68. E. L. Yee, R. J. Cave, K. L. Guyer, P. D. Tyma, and M. J. Weaver, "A survey of ligand effects upon the reaction entropies of some transition metal redox couples." *J. Am. Chem. Soc.*, **101**, 1131 (1979).
69. J. E. J. Schmitz and A. H. Montree, "Determination of the reaction entropy of a quasi-reversible redox reaction with cyclic voltammetry." *Anal. Chem.*, **57**, 371 (1985).
70. X.-G. Yang, T. Liu, Y. Gao, S. Ge, Y. Leng, D. Wang, and C.-Y. Wang, "Temperature Modulation for Extreme Fast Charging of Lithium-Ion Batteries." *Joule*, **3**, 3002 (2019).
71. S. W. Lee, Y. Yang, H.-W. Lee, H. Ghasemi, D. Kraemer, G. Chen, and Y. Cui, "An electrochemical system for efficiently harvesting low-grade heat energy." *Nat. Commun.*, **5**, 3942 (2014).
72. T. Y. George, E. F. Kerr, N. O. Haya, A. M. Alfaraidi, R. G. Gordon, and M. J. Aziz, "Size and Charge Effects on crossover of flow battery reactants evaluated by quinone permeabilities through nafion." *J. Electrochem. Soc.*, **170**, 040509 (2023).
73. C. Costentin, M. Robert, and J.-M. Savéant, "Adiabatic and non-adiabatic concerted proton–electron transfers. Temperature effects in the oxidation of intramolecularly hydrogen-bonded phenols." *J. Am. Chem. Soc.*, **129**, 9953 (2007).
74. C. Costentin, M. Robert, and J.-M. Savéant, "Reorganization energies and pre-exponential factors in the one-electron electrochemical and homogeneous oxidation of phenols coupled with an intramolecular amine-driven proton transfer." *Phys. Chem. Chem. Phys.*, **12**, 13061 (2010).
75. C. Costentin, V. Hajji, C. Louault, M. Robert, and J.-M. Savéant, "Concerted proton–electron transfers. Consistency between electrochemical kinetics and their homogeneous counterparts." *J. Am. Chem. Soc.*, **133**, 19160 (2011).
76. S. Ferro and A. De Battisti, "The 5-V window of polarizability of fluorinated diamond electrodes in aqueous solutions." *Anal. Chem.*, **75**, 7040 (2003).
77. B. H. Robb, S. E. Waters, and M. P. Marshak, "Evaluating aqueous flow battery electrolytes: a coordinated approach." *Dalton Transactions*, **49**, 16047 (2020).
78. Y. K. Zeng, T. S. Zhao, X. L. Zhou, J. Zou, and Y. X. Ren, "A hydrogen-ferric ion rebalance cell operating at low hydrogen concentrations for capacity restoration of iron-chromium redox flow batteries." *Journal of Power Sources*, **352**, 77 (2017).
79. R. M. Wittman, M. L. Perry, T. N. Lambert, B. R. Chalamala, and Y. Preger, "Perspective—On the need for reliability and safety studies of grid-scale aqueous batteries." *J. Electrochem. Soc.*, **167**, 090545 (2020).